UNCLASSIFIED

[redacted]

Copy 537

NASA TM X-90

NASA TM X-90

TECHNICAL MEMORANDUM

X-90

THE DAMPING IN PITCH OF BLUFF BODIES OF REVOLUTION AT MACH NUMBERS FROM 2.5 TO 3.5

By Benjamin H. Beam and C. Ernest Hedstrom

Ames Research Center
Moffett Field, Calif.

CL... ...N CHANGED TO UNCLASSIFIED
BY ... OF NASA CLASSIF... CHANGE
N... ES. CHANGE NO. 2-9-24 EFF. 10/19/70

NATIONAL AERONAUTICS AND SPACE ADMINISTRATION

WASHINGTON October 1959

[redacted]

UNCLASSIFIED

5523

[redacted]

NATIONAL AERONAUTICS AND SPACE ADMINISTRATION

TECHNICAL MEMORANDUM X-90

THE DAMPING IN PITCH OF BLUFF BODIES OF REVOLUTION AT MACH NUMBERS FROM 2.5 TO 3.5*

By Benjamin H. Beam and C. Ernest Hedstrom

SUMMARY

Results of supersonic wind-tunnel tests to measure the pitching moment and the damping in pitch derivatives of two bluff bodies of revolution at supersonic speeds are presented.

One bluff body was comprised of a parabolic forebody and a cone-shaped afterbody. The other bluff body consisted of a flattened forebody with three variations of corner radii and two cone-shaped afterbodies.

Tests were conducted at various longitudinal locations of the moment center for each body of revolution. Data were obtained at Mach numbers of 2.5, 3.0, and 3.5; both with and without artificially induced boundary-layer transition and at two values of Reynolds number. The results presented herein are compared with values estimated by impact theory. Reasonable agreement with theory was obtained for the body of revolution having a parabolic forebody. The damping in pitch of the body of revolution having a flattened forebody was destabilizing at zero angle of attack and sideslip and did not agree with impact theory.

INTRODUCTION

A number of investigators (refs. 1 and 2) have studied the dynamic motion of bluff bodies traveling at high speeds on descending paths through the atmosphere. It is found that the amplitude of the initial dynamic motion is convergent for vehicles with static aerodynamic stability, irrespective of the magnitude of the damping derivatives. Thus, initially large oscillation amplitudes which arise from misalinement of the axis of the vehicle with the flight path will become smaller as the vehicle descends. In general, this situation applies as long as the dynamic pressure is increasing with time. The increasing atmospheric

*Title, Unclassified

[redacted]

[redacted]

density as the vehicle descends leads to progressively increasing dynamic pressure even though the vehicle speed is dropping. At some point in its trajectory, however, the vehicle decelerates sufficiently that the dynamic pressure no longer increases, and at this point the damping in pitch derivative, $C_{m_q} + C_{m_{\dot{\alpha}}}$, becomes very important to the dynamic stability. In this region theory indicates that the oscillations of the vehicle will or will not eventually converge to zero accordingly as the stability parameter (ref. 1)

$$\xi = C_D - C_{L_\alpha} + \left(\frac{D}{\sigma}\right)^2 \left(C_{m_q} + C_{m_{\dot{\alpha}}}\right)$$

is negative or positive. Since C_D is always positive and C_{L_α} is generally low and can be negative for bluff shapes, the convergence of dynamic motions in this region of the trajectory depends to a large extent on negative (or stabilizing) values of the dynamic stability derivative $C_{m_q} + C_{m_{\dot{\alpha}}}$.

The only method which lends itself readily to the calculation of the damping derivatives of bluff shapes at supersonic speeds is the Newtonian impact theory (ref. 3, for example) which is a greatly oversimplified theory especially in regard to details of the flow. Recent experimental tests (refs. 4, 5, 6, and 7) have been directed at providing quantitative data on these bluff configurations, and more reliable methods of estimating their characteristics.

The purpose of this report is to present values of the static and dynamic stability derivatives measured on an oscillation mechanism in a wind tunnel for two bluff bodies of revolution at Mach numbers from 2.5 to 3.5. The data are compared with values estimated using Newtonian impact theory.

SYMBOLS

The moment reference center for various configurations is shown in figures 1 and 2.

C_D drag coefficient, $\dfrac{\text{drag}}{(1/2)\rho V^2 S}$

C_{L_α} rate of change of lift coefficient with angle of attack, $\dfrac{\partial}{\partial\alpha}\left[\dfrac{\text{lift}}{(1/2)\rho V^2 S}\right]$

[redacted]

C_m pitching-moment coefficient, $\frac{\text{pitching moment}}{(1/2)\rho V^2 SD}$

C_{m_α} $\frac{\partial C_m}{\partial \alpha}$

C_{m_q} $\frac{\partial C_m}{\partial (qD/V)}$

$C_{m_{qi}}$ value of C_{m_q} from Newtonian impact theory

$C_{m_{\dot{\alpha}}}$ $\frac{\partial C_m}{\partial (\dot{\alpha} D/V)}$

$(C_{m_q} + C_{m_{\dot{\alpha}}})_h$ value of $(C_{m_q} + C_{m_{\dot{\alpha}}})$ due to hysteresis in pitching moment

D diameter of the base of the forebody

q pitching velocity

R Reynolds number referred to diameter of the base of the forebody

S area of the base of forebody

t time

V velocity

W work

X axial location of moment center behind nose

α angle of attack

α_m mean angle of attack, or steady angle of attack about which oscillatory pitching motions take place, deg

α_o maximum oscillatory component of angle of attack

$\pm\alpha_h$ assumed limiting angles of attack of pitching-moment hysteresis (see fig. 12)

β angle of sideslip

[redacted]

ξ	dynamic stability parameter, $C_D - C_{L_\alpha} + \left(\frac{D}{\sigma}\right)^2 \left(C_{m_q} + C_{m_{\dot\alpha}}\right)$
σ	radius of gyration in pitch of vehicle
ρ	mass density of air
ω	circular frequency of oscillation
$\Delta(\ )$	incremental value of a quantity ( )
$(\dot{\ })$	derivative of a quantity with respect to time, $\frac{d(\ )}{dt}$

APPARATUS AND MODELS

Test Facility

The experimental data were obtained in the 8- by 7-foot supersonic test section of the Ames Unitary Plan wind tunnel. This test section is capable of continuous variations of nominal Mach number from 2.5 to 3.5 and of a stagnation pressure from 2 to 28 pounds per square inch absolute.

Models

The geometric characteristics of the two bodies of revolution used in this investigation are shown in figures 1 and 2. The body of revolution having a paraboloid forebody is shown in figure 1. A sketch of the body of revolution having a flattened forebody is shown in figure 2. Tests were also conducted on several variations in the basic shape of this latter body, and these variations are shown in figures 2(b) and 2(c). Photographs of this body on the oscillation mechanism in the wind-tunnel test section are shown in figure 3.

All forebodies and afterbodies were made of plastic laminated glass cloth and were attached to an alluminum alloy base plate and support tube. After filling, sanding, and buffing all indentations, the outer surfaces were given a flat white enamel finish. The inner surface of the support tube to which all components were attached was machined to mate with the oscillation mechanism. The location of the moment center was varied by mating the oscillation mechanism to the support tube at different longitudinal positions.

[redacted]

[redacted]

Oscillation Apparatus

The oscillation apparatus described in reference 8 was used in this investigation. This apparatus consisted of a dynamic balance and the necessary supporting electronic equipment to establish a steady-state forced oscillation of the model. The moments and deflections within the balance were measured electronically, and from the measured values the desired static and dynamic derivatives were evaluated. The model oscillation was of a single degree of freedom having a maximum amplitude of $\pm 1\text{-}1/2^{\circ}$. Deflection galvanometers indicated visually the steady-state values of oscillation amplitude and input torque required to maintain oscillation. The oscillation frequency depended upon the natural oscillation frequency of the model on the crossed-flexure spring support within the balance and had a frequency of approximately 10 cycles per second. An electronic counter indicated visually the frequency of the model oscillations.

For some of the tests with the body of revolution having a flattened forebody, four ±4 pounds per square inch miniature electrical pressure gages were installed in the afterbody at the locations shown in figure 2(a). The output of these cells was recorded on magnetic tape.

TESTS

Data were taken at Mach numbers of 2.5, 3.0, and 3.5 through a range of angles of attack at zero sideslip angle for all configurations. Some data were also taken through a range of angles of sideslip at zero angle of attack. The Reynolds number for the tests was 3 million except for measurements of the effect of scale on the body of revolution having a flattened forebody, for which tests were made at a Reynolds number of 2 million.

Surface roughness was applied to the body of revolution having a flattened forebody as a means of artificially inducing transition from laminar to turbulent flow over the forebody. The increased surface roughness was obtained by applying commercial table salt to a prepared adhesive surface with about 80-percent particle density. The entire front face including the corner but excluding the base flare was covered in this way.

[redacted]

[redacted]

CORRECTIONS TO DATA

Tare corrections to the measured values of damping were determined from measurements of the damping with the wind tunnel evacuated and at zero airspeed immediately prior to a series of test runs on a particular configuration. These corrections, which account for the mechanical friction effects in the model and oscillation mechanism, were then subtracted from the values of damping derivative measured with the wind on. The magnitude of this correction to $C_{m_q} + C_{m_{\dot{\alpha}}}$ was approximately 0.04 for all configurations.

A correction was applied to the measured values of C_{m_α} to account for the change in spring constant of the flexure pivots in the oscillation mechanism under the heavy drag load encountered on the models. This correction, which is in the nature of a drag interaction with C_{m_α}, was computed from known drag forces on these models and the effect of the resulting compressive forces on the spring constant of crossed flexure pivots. The magnitude of this correction to C_{m_α} varied somewhat with Mach number and Reynolds number but was approximately 0.022 per radian for the body of revolution having a paraboloid forebody and 0.026 per radian for the body of revolution having a flattened forebody. This resulted in smaller absolute values of C_{m_α}.

Random errors in the data resulting from wind-tunnel turbulence, buffeting of the model, and errors in the visual reading of the deflection galvanometers were largely averaged out by repeated measurements. For each test condition two readings were taken at slightly different maximum oscillation amplitudes from 1° to $1\text{-}1/2^\circ$.

Corrections were applied to Mach number and angle of attack based on stream survey data of the test section indicating local Mach number and flow angularity in the test region.

RESULTS AND DISCUSSION

The results of wind-tunnel tests on two bluff bodies of revolution are presented in figures 4 through 11. As mentioned in the introduction, one of the objectives of these tests was to compare the experimental results with values estimated from theory for bodies of this type. Since the Newtonian impact theory has been shown to be fairly applicable to bluff bodies in the range of Mach number considered in this report (ref. 9), and since it is possibly the only theory that can be readily applied to these shapes, it has been used as a standard of comparison.

[redacted]

In the discussion that follows it will be shown that very different agreement was obtained in making this comparison with impact theory for the two bodies considered.

Body of Revolution Having Paraboloid Forebody

The experimental data and calculated values of static stability and damping in pitch derivatives for the body of revolution having a paraboloid forebody (fig. 1) are shown in figure 4. Over the relatively small range of mean angle of attack, α_m, over which tests were conducted, the impact theory indicates no variation in these derivatives with α_m. This is verified in general by the trend of the experimental data except at a Mach number of 3.5 with the most forward moment center position (fig. 4). In addition, the afterbody configuration is seen to have a negligible influence on the measured values of the derivatives, as expected from impact theory (with one exception noted for a Mach number of 3.5 and a moment center located 0.292D aft of the nose). The longitudinal stability derivatives for a mean angle of attack of zero and for various sideslip angles are shown in figure 5. These data show that the static stability and damping in pitch derivatives are approximately independent of sideslip angle for this configuration.

When the data for a mean angle of attack of zero are cross plotted with location of the moment center as in figure 6, the experimental values of the static stability derivative C_{m_α} are found to agree closely with values calculated from impact theory. The experimental values of damping in pitch derivative $C_{m_q} + C_{m_{\dot{\alpha}}}$ are from 15 to 50 percent lower than values calculated from impact theory. The trend of the damping derivative data with location of the moment center for both Mach numbers of 2.5 and 3.5 is approximately as indicated by theory. From these data it is concluded that the Newtonian model of the flow about the body of revolution having a paraboloid forebody is a fair guide in estimating the dynamic stability derivatives in the range of Mach numbers from 2.5 to 3.5.

Body of Revolution Having Flattened Forebody

The basic data for the second body of revolution considered is presented in figure 7. For this configuration (F_2A_2 as shown in fig. 2(a)) the experimental values of damping in pitch derivative became positive, or destabilizing, for mean angles of attack near zero. This effect is not indicated by the impact theory, calculated values of which are also shown in figure 7. Experimental values of the static stability derivative, C_{m_α}, more nearly agree with calculated values, but here also there is a noticeable variation with angle of attack in the experimental data.

Furthermore, the longitudinal derivative data for a mean angle of attack of zero and for various sideslip angles, presented in figure 8, show a marked variation with sideslip angle. A cross plot of the measured values of the derivatives at zero angle of attack for this body, similar to that shown in figure 6 for the previous body, is presented in figure 9. The differences between theory and experiment are apparent.

The dynamic instability at low angles of attack and the lack of agreement with theory for this shape is a possible source of concern for similar configurations in flight. These considerations led to an investigation of the factors which might cause large variations in damping coefficient, and in the course of this study several variations in shape from the basic body of revolution having a flattened forebody were tested.

On the assumption that flow separation or some related boundary-layer phenomena could be occurring at the small radius corner, or "shoulder," two forebodies having different corner radii were tested. On one the corner radius was twice that of the basic configuration and on the other the corner radius was half that of the basic configuration (see fig. 2(b)). These variations were selected because the pressure distributions calculated from impact theory are known to be particularly in error in the vicinity of a sharp corner. Calculations including an allowance for "centrifugal forces" (see ref. 3, for example) indicated that the pressure coefficients could become negative at the corner and depend strongly on the corner radius. From these and other considerations it was expected that variations in corner radius might lead to distinct differences in the flow about the bodies and the measured values of damping coefficient, which would account for the anomalous effects observed in figure 7.

The measured effects of these changes in the shape of the forebody are shown in figure 10. It can be seen that there were some effects of forebody corner radius on the damping derivative $C_{m_q} + C_{m_{\dot{\alpha}}}$, but that the general character of the variations with angle of attack was not altered materially.

Variations in the afterbody shape from the large afterbody A_1 to the small afterbody A_2 and no afterbody A_3 (fig. 2(c)) are shown in figure 10 to result in marked differences in the damping derivative $C_{m_q} + C_{m_{\dot{\alpha}}}$. This is surprising since the entire afterbody should be in the wake of the forebody with very little influence on the stability because of the low static pressure in this region. The impact theory is of no use in understanding this situation since, where the entire afterbody is sheltered from the stream by the forebody, zero base pressure is indicated. Time histories of the variations in base pressure were measured with pressure cells in the afterbody and the base of the forebody (see fig. 2(c)). Analysis of records of these measurements indicated only random variations in base pressure coefficient having mean values less than 0.004.

Data on the effects of variations in Reynolds number and artificially induced transition are presented in figure 11 for the flattened forebody configuration with medium forebody radius and large afterbody. From shadowgraph studies (not published in this report) it was known that at a Reynolds number of 2 million the boundary layer was completely laminar to the separation point at the base of the forebody where it mixed with the slower moving air in the wake. With roughness applied the boundary layer was very thick and turbulent at the corner on the forebody. These changes in Reynolds number and surface roughness resulted in some distinct differences in values of the damping derivative near zero angle of attack (fig. 11) but in all cases some positive values of $C_{m_q} + C_{m_{\dot{\alpha}}}$ were observed. These data show that changes in the condition of the boundary layer over the forebody are not of major importance in accounting for the observed instability.

Analysis of Damping Due to Hysteresis

Although it is apparent from the above discussion that the particular mechanism which results in positive values of $C_{m_q} + C_{m_{\dot{\alpha}}}$ is not well understood, there is a consistent feature of these data which is of considerable importance. In figure 4 it may be noted that the static stability derivative C_{m_α} for the body of revolution having a paraboloid forebody is quite constant with variations in mean angle of attack. In figures 7, 10, and 11 it is noted that the variations in C_{m_α} with mean angle of attack for the body of revolution having a flattened forebody are much less regular. In fact, in nearly every case where $C_{m_q} + C_{m_{\dot{\alpha}}}$ is seen to become more positive, C_{m_α} becomes more negative. Evidently there is a relation between variations in the two derivatives, and the manner in which they are related is suggested as follows.

In figure 12(a) a typical variation of C_m with α is shown such as might correspond with the variation of C_{m_α} shown in figure 7. The solid line represents the time-averaged experimental variation whereas the dotted lines represent the probable instantaneous variation of C_m with α. The hysteresis loop results where there is a lag in the establishment of the pitching moment following a change in angle of attack. The different variations in C_m' and C_m'' with increasing and decreasing α may be represented another way as in figure 12(b). Here C_{m_α} can be represented by two curves, C_{m_α}' representing the variation of the static stability derivative with increasing angle of attack, and C_{m_α}'' that with decreasing angle of attack.

The pitching moment acting through an increment of angle of attack represents an increment of work. Thus:

[redacted]

$$dW = \frac{1}{2} \rho V^2 SDC_m \, d\alpha = \frac{1}{2} \rho V^2 SDC_{m_\alpha} \alpha \, d\alpha \tag{1}$$

and the net work over a cycle is:

$$\Delta W = \frac{1}{2} \rho V^2 SD \left(\int_{-\alpha}^{+\alpha} C_{m_\alpha}{}' \alpha \, d\alpha + \int_{+\alpha}^{-\alpha} C_{m_\alpha}{}'' \alpha \, d\alpha \right) \tag{2}$$

$$= \frac{1}{2} \rho V^2 SD \int_{-\alpha}^{+\alpha} \delta C_{m_\alpha} \alpha \, d\alpha \tag{3}$$

where $\delta C_{m_\alpha} = C_{m_\alpha}{}' - C_{m_\alpha}{}''$. A consideration of the variation of δC_{m_α} with α, illustrated graphically in figure 12(c), indicates that this variation will have an approximately sinusoidal shape between the limiting angles of the hysteresis loop. Thus, on the assumption that the principal component is sinusoidal, δC_{m_α} in fig. 12(c) can be represented by

$$\delta C_{m_\alpha} \approx -\Delta C_{m_\alpha} \sin \frac{\pi \alpha}{\alpha_h}, \qquad -\alpha_h \leqq \alpha \leqq \alpha_h \tag{4}$$

and

$$\Delta W \approx -\rho V^2 SD \Delta C_{m_\alpha} \frac{{\alpha_h}^2}{\pi} \tag{5}$$

where ΔC_{m_α} is the maximum value of δC_{m_α}, and can be taken as the experimentally observed difference in C_{m_α} between 0° and $\pm 2^\circ$ angle of attack in figure 7 for example.

It is desirable to interpret the work per cycle from hysteresis in terms of an equivalent damping derivative. For an assumed constant equivalent damping derivative, the work can be calculated from

$$dW = \frac{1}{2} \rho V^2 SD \left(\frac{\dot{\alpha} D}{V} \right) \left(C_{m_q} + C_{m_{\dot{\alpha}}} \right)_h d\alpha \tag{6}$$

[redacted]

[redacted]

and since $\left(C_{m_q} + C_{m_{\dot{\alpha}}}\right)_h$ is considered a constant coefficient over the cycle,

$$\Delta W = \rho VSD^2 \left(C_{m_q} + C_{m_{\dot{\alpha}}}\right)_h \int_{-\alpha}^{+\alpha} \dot{\alpha}\, d\alpha \tag{7}$$

The variation of α with time can be considered very nearly sinusoidal even with the nonlinearities present in the pitching moment

$$\alpha = \alpha_o \sin \omega t \tag{8}$$

$$\Delta W = \rho VSD^2 \left(C_{m_q} + C_{m_{\dot{\alpha}}}\right)_h \int_{-\pi/2\omega}^{\pi/2\omega} \dot{\alpha}^2 dt \tag{9}$$

$$= \rho VSD^2 \left(C_{m_q} + C_{m_{\dot{\alpha}}}\right)_h \pi\omega\alpha_o{}^2 \tag{10}$$

The work done from hysteresis (eq. (5)) can then be equated to the work resulting from an equivalent damping derivative (eq. (10)), resulting in

$$\left(C_{m_q} + C_{m_{\dot{\alpha}}}\right)_h = -\frac{2}{\pi^2}\left(\frac{V}{\omega D}\right)\Delta C_{m_\alpha}\left(\frac{\alpha_h}{\alpha_o}\right)^2 , \qquad \alpha_h \leqq \alpha_o \tag{11}$$

Thus, if one wished to modify the values of damping coefficient, $C_{m_{qi}}$, estimated from impact theory to allow for a hysteresis as above, the complete expression becomes

$$C_{m_q} + C_{m_{\dot{\alpha}}} = C_{m_{qi}} + \left(C_{m_q} + C_{m_{\dot{\alpha}}}\right)_h \tag{12}$$

$$= C_{m_{qi}} - \frac{2}{\pi^2}\left(\frac{V}{\omega D}\right)\Delta C_{m_\alpha}\left(\frac{\alpha_h}{\alpha_o}\right)^2$$

[redacted]

The above analysis, although approximate, emphasizes several points. One is that an incremental negative change in C_{m_α}, or a "pitch down characteristic" can lead to dynamic instability where hysteresis is present. The experimental data in figures 7, 8, 10, and 11 clearly show the relation between negative incremental changes in C_{m_α} and positive incremental changes in $C_{m_q} + C_{m_{\dot\alpha}}$. From this it might be thought that wind-tunnel force data on the variation of C_m with α would immediately reveal this type of instability. Actually, this latter view must be accepted with considerable reservation if at all because the uncertainties in wind-tunnel force data can lead to ambiguous or erroneous interpretations. Experimental pitching-moment data from reference 7 and the data of this report for the same configuration - the body of revolution having a flattened forebody and small afterbody - are presented in figure 13. The nonlinearities in the data from oscillation tests which account for the dynamic instability due to hysteresis are hardly apparent when presented in this way, and are within the accuracy of the static tests. Thus, with the uncertainties present in wind-tunnel data, it can be concluded that an apparently linear variation of C_m with α is not sufficient assurance that instability due to hysteresis is not present. Alternatively, if the nonlinearities are large enough to be obvious in the static force data this could be expected to have profound effects on dynamic stability where hysteresis is present.

Values of ΔC_{m_α} from the experimental data, taken as the maximum incremental change in C_{m_α} from the oscillation data (e.g., $\Delta C_{m_\alpha} \approx -0.04$ for $M = 3.5$ in fig. 7), when inserted in equation (11) along with appropriate test variables result in positive increments of about ±0.15 in $C_{m_q} + C_{m_{\dot\alpha}}$. This magnitude is somewhat lower but of the same order as that observed experimentally, even though the analysis is not rigorous because of the assumed equation (4) regarding the shape of the hysteresis loop. Thus a second point is that useful estimates of the damping resulting from hysteresis in pitching moment could be made using this analysis or similar analyses which consider the change in work due to hysteresis.

A third point involves a consideration of the implications of these data on the motion of a vehicle in free flight. It has been shown that the dynamic stability of small amplitude oscillations about an equilibrium angle of attack can vary markedly with the equilibrium angle of attack. It has also been shown that the dynamic stability at any given angle of attack can vary markedly with sideslip angle. The dynamic stability derivative $C_{m_q} + C_{m_{\dot\alpha}}$ in general is thus a function of both α and β. For a body of revolution in free flight, the distinction between α and β is purely arbitrary and in all likelihood oscillations will occur in both planes at once, which can be visualized as a point on the nose of the vehicle spiraling around the flight path. The result is that the apparent damping of the longitudinal motion will be influenced not only by its amplitude but also by the amplitude of the directional motion, and vice versa. With reference to the body of revolution having a flattened forebody, it is the opinion of the authors that reliable estimates of the details of the oscillatory motion in free flight under these conditions cannot be made by use of the simplified equations of motion and the data of this report because of the strong nonlinearity indicated in the data. On the other hand, the body of revolution having a paraboloid forebody exhibits acceptable characteristics for analysis of its oscillatory motion on the basis of linearized equations, and the data of this report along with appropriate values of C_D and C_{L_α} could be used in assessing its stability.

SUMMARY OF RESULTS

The results of wind-tunnel oscillation tests on two bodies of revolution at Mach numbers from 2.5 to 3.5 can be summarized as:

1. For the body of revolution having a paraboloid forebody, the static stability and damping in pitch showed little variation with angle of attack and sideslip and was in fair agreement with impact theory.

2. For the body of revolution having a flattened forebody, $C_{m_q} + C_{m_{\dot\alpha}}$ was positive, or destabilizing, near zero angle of attack and zero sideslip, was strongly dependent on α and β, and did not agree with impact theory. The observed variations in damping were strongly influenced by the afterbody configuration.

3. A study of the experimental data indicates that a relation exists between variations in static stability and damping in pitch. An explanation of this effect on the basis of hysteresis is suggested in this report.

Ames Research Center
National Aeronautics and Space Administration
Moffett Field, Calif., May 29, 1959

REFERENCES

1. Allen, H. Julian: Motion of a Ballistic Missile Angularly Misaligned With the Flight Path Upon Entering the Atmosphere and Its Effect Upon Aerodynamic Heating, Aerodynamic Loads, and Miss Distance. NACA TN 4048, 1957.

2. Friedrich, Hans R., and Dore, Frank J.: The Dynamic Motion of a Missile Descending Through the Atmosphere. Jour. Aero. Sci., vol. 22, no. 9, Sept. 1955, pp. 628-632, 638.

3. Grimminger, G., Williams, E. P., and Young, G. B. W.: Lift on Inclined Bodies of Revolution in Hypersonic Flow. Jour. Aero. Sci., vol. 17, no. 11, Nov. 1950, pp. 675-690.

4. Coltrane, Lucille C.: Investigation of Two Bluff Shapes in Axial Free Flight Over a Mach Number Range From 0.35 to 2.15. NACA RM L58A16, 1958.

5. Buell, Donald H., and Johnson, Norman S.: An Experimental and Analytical Investigation of the Dynamics of Two Blunt Bodies at Subsonic Speeds. NASA MEMO X-18, 1959.

6. Short, Barbara, and Sommer, Simon C.: Some Measurements of the Dynamic and Static Stability of Two Blunt-Nosed, Low-Fineness-Ratio Bodies of Revolution in Free Flight at $M = 4$. NASA MEMO X-20, 1959.

7. DeRose, Charles E.: Normal-Force and Pitching-Moment Characteristics of Two Blunt-Nosed Re-entry Type Bodies From $M = 2.4$ to $M = 4.0$. NASA MEMO 2-4-59A, 1959.

8. Beam, Benjamin H.: A Wind-Tunnel Test Technique for Measuring the Dynamic Rotary Stability Derivatives at Subsonic and Supersonic Speeds. NACA Rep. 1258, 1956. (Supersedes NACA TN 3347)

9. Machell, Reginald M., and O'Bryant, William T.: An Experimental Investigation of the Flow Over Blunt-Nosed Cones at a Mach Number of 5.8. GALCIT Memo. 32, June 15, 1956.

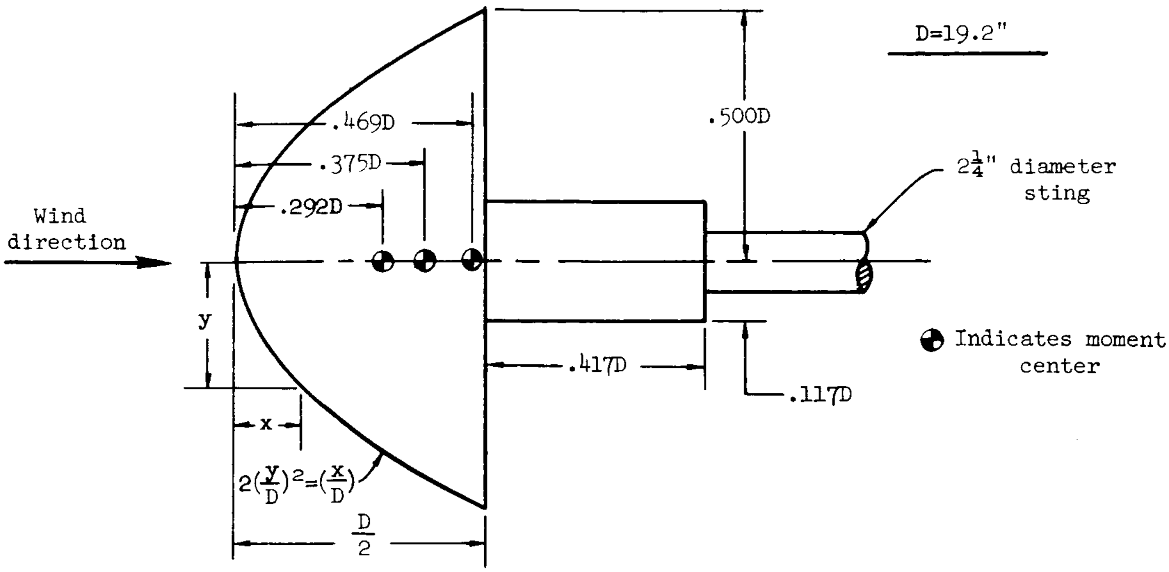

(a) Parabolic forebody with no afterbody.

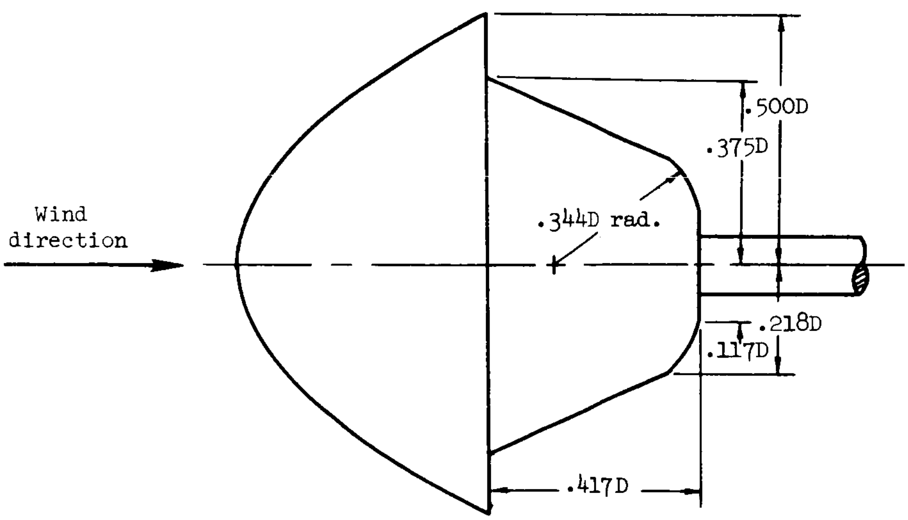

(b) Parabolic forebody with afterbody.

Figure 1.- Sketch of body of revolution having paraboloid forebody.

[redacted]

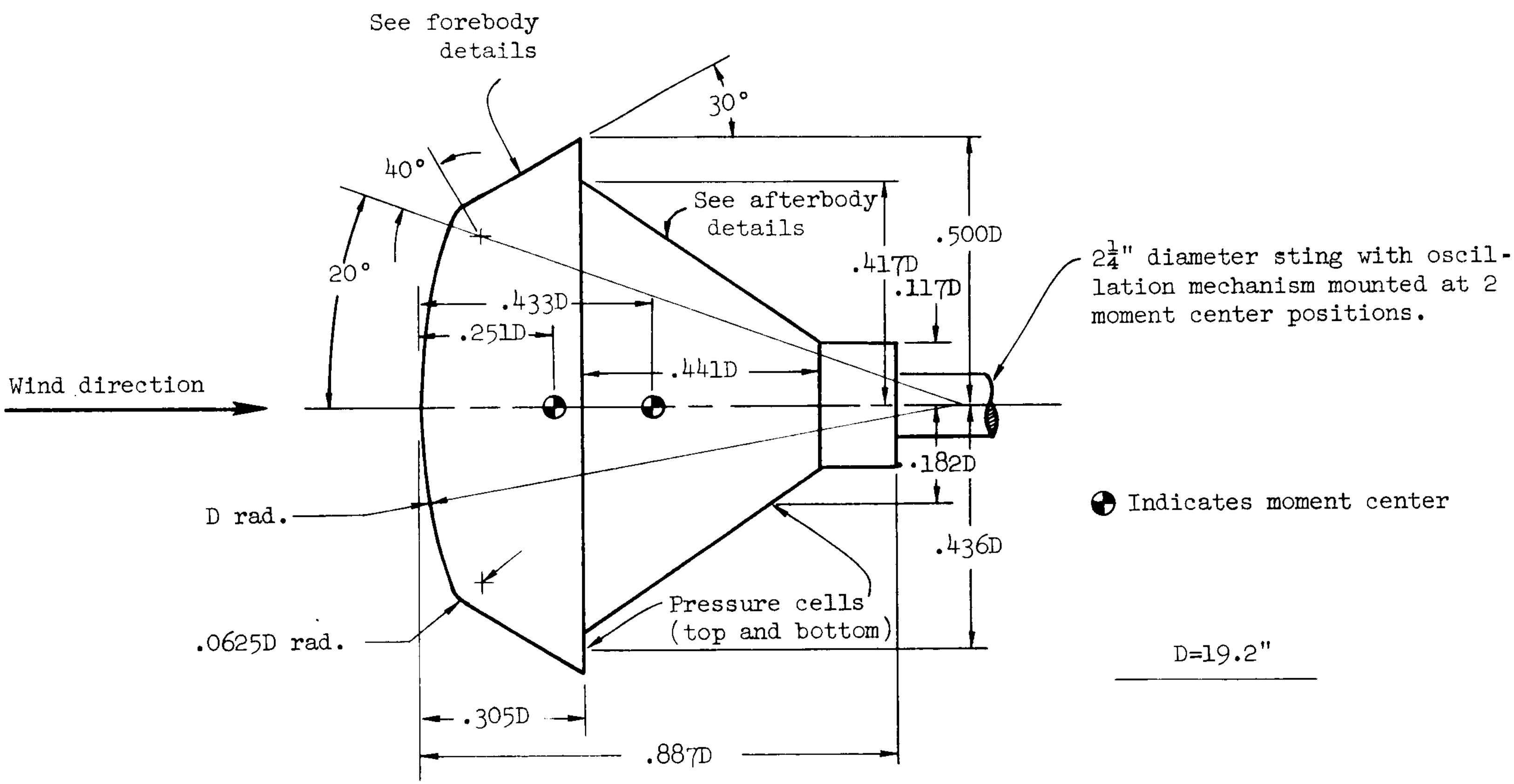

(a) Basic configuration, F_2A_2.

Figure 2.- Sketch of body of revolution having flattened forebody.

[redacted]

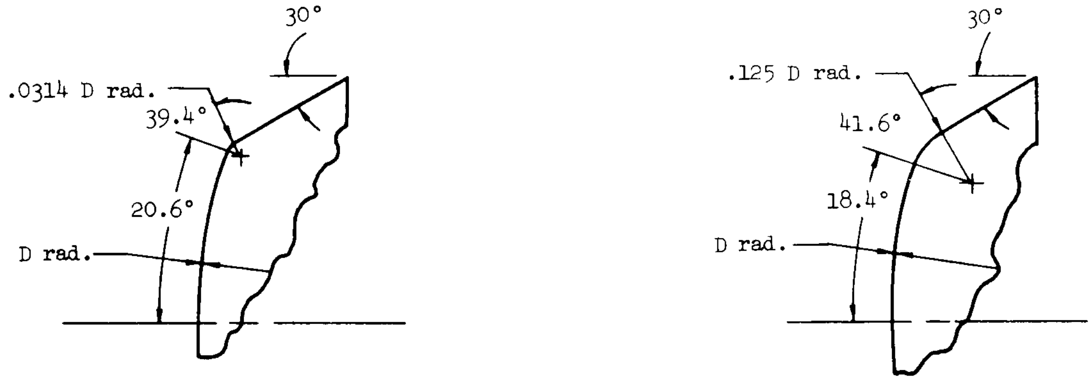

Small corner radius-F1

Large corner radius-F3

(b) Details of forebody variations, D = 19.2 inches.

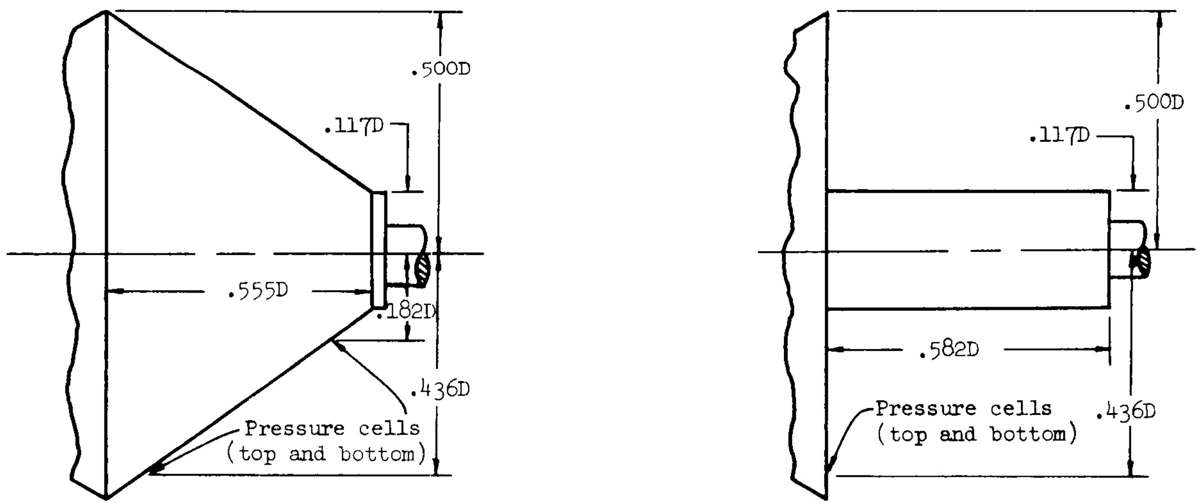

Large afterbody-A1

No afterbody-A3

(c) Details of afterbody variations, D = 19.2 inches.

Figure 2.- Concluded.

[redacted]

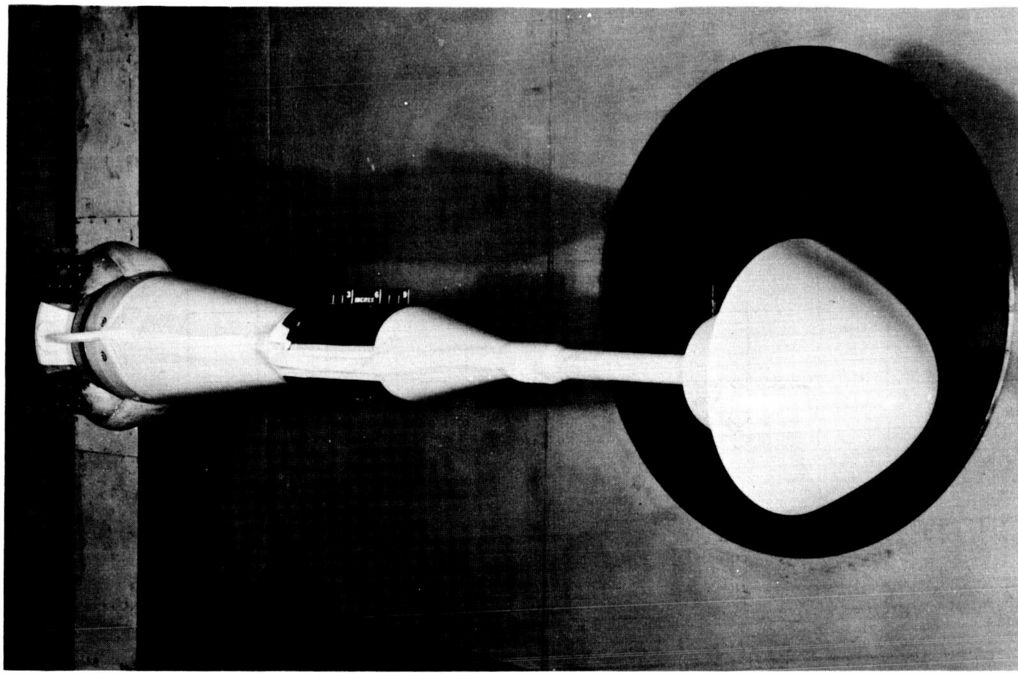

A-21846

(a) Front quarter view.

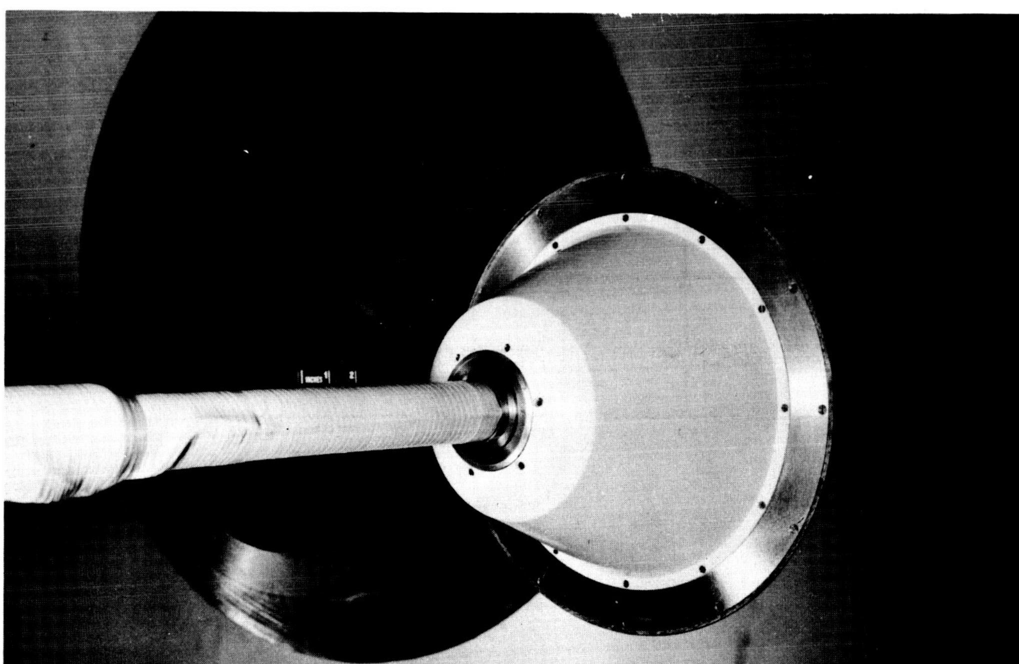

A-21847

(b) Rear quarter view.

Figure 3.- Photograph of model (parabolic forebody with afterbody) in test section.

[redacted]

[redacted]

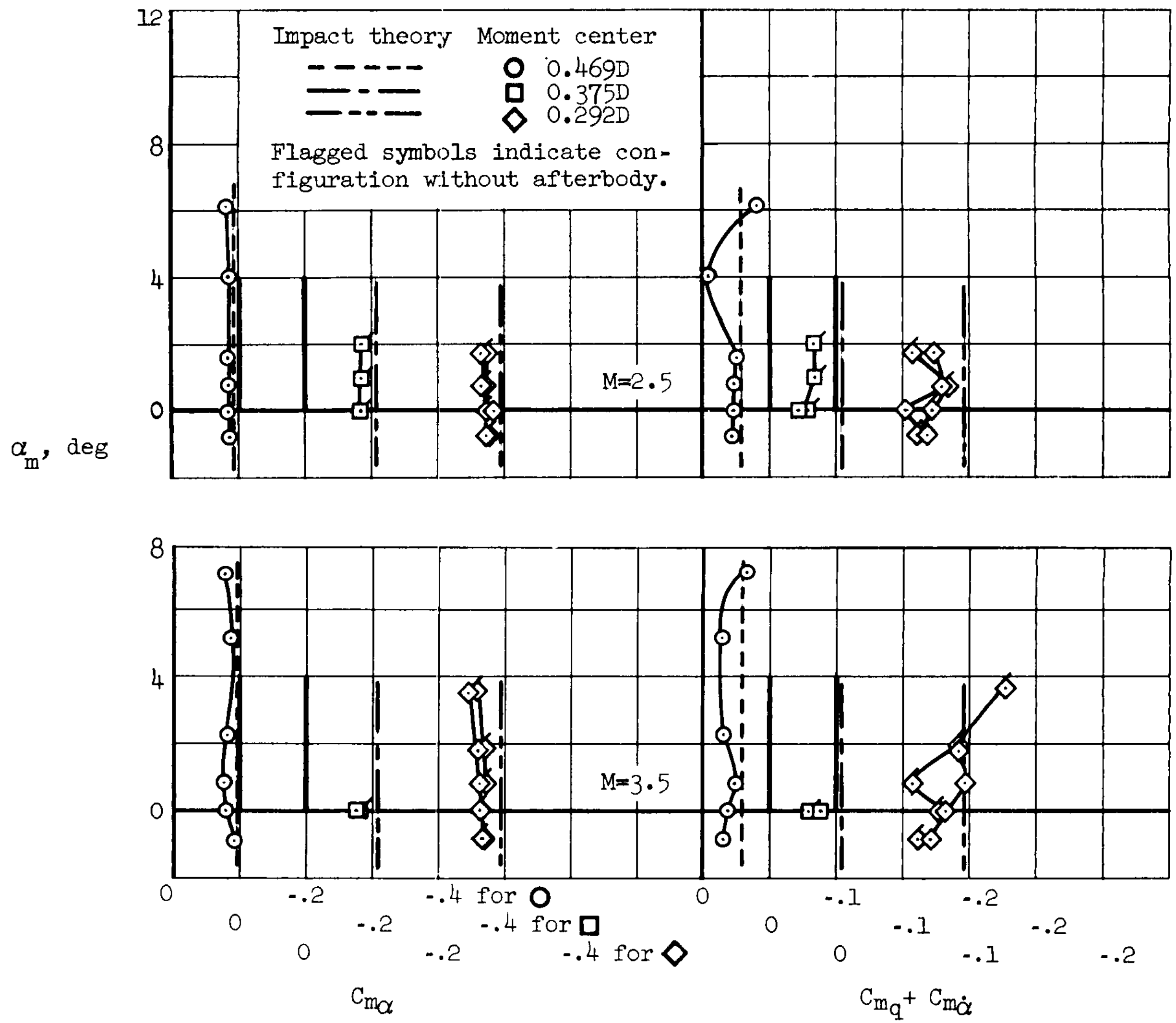

Figure 4.- Basic data on parabolic forebody with afterbody; three moment center positions, two Mach numbers with and without afterbody.

[redacted]

[redacted]

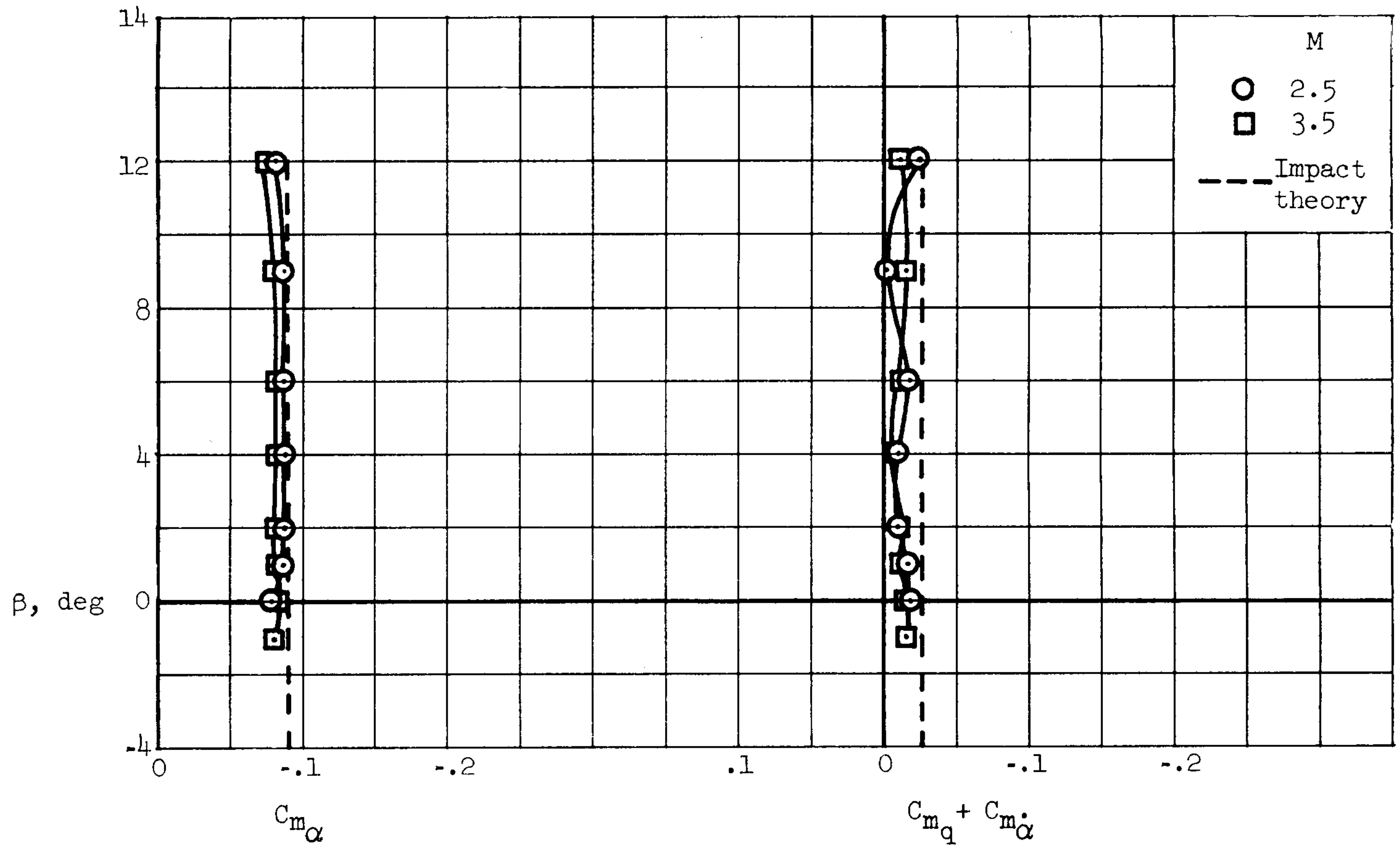

Figure 5.- Effect of variations in sideslip angle on the longitudinal dynamic stability derivatives at zero angle of attack for the body of revolution having a parabolic forebody with afterbody; moment center = 0.469D.

[redacted]

[redacted]

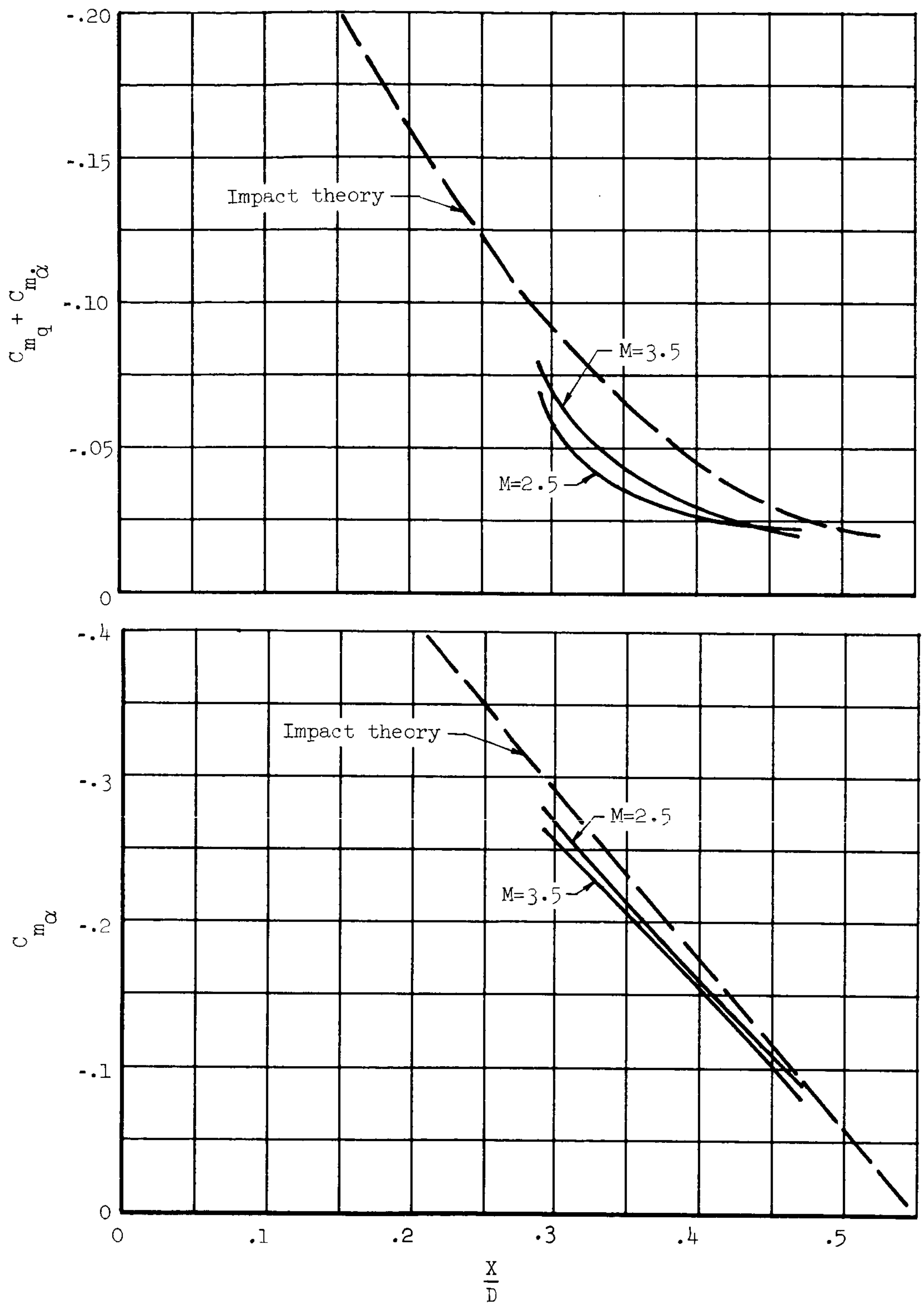

Figure 6.- The variation of static stability and damping in pitch with the location of the pitching axis on parabolic forebody with afterbody at $\alpha_m = 0^\circ$.

[redacted]

[redacted]

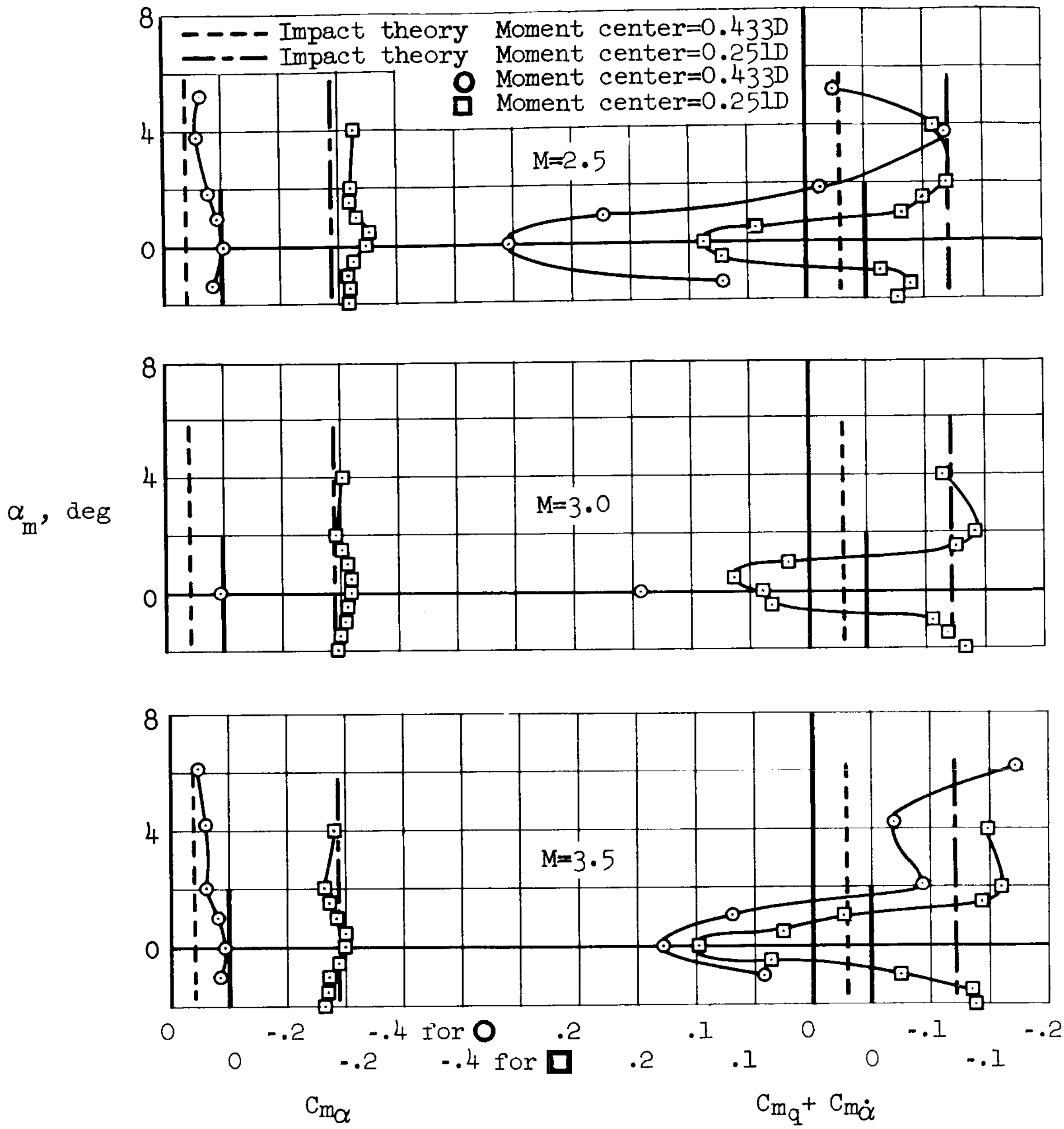

Figure 7.- Basic data on body of revolution having flattened forebody; medium forebody with small afterbody (F_2A_2) at two moment center positions and at three Mach numbers.

[redacted]

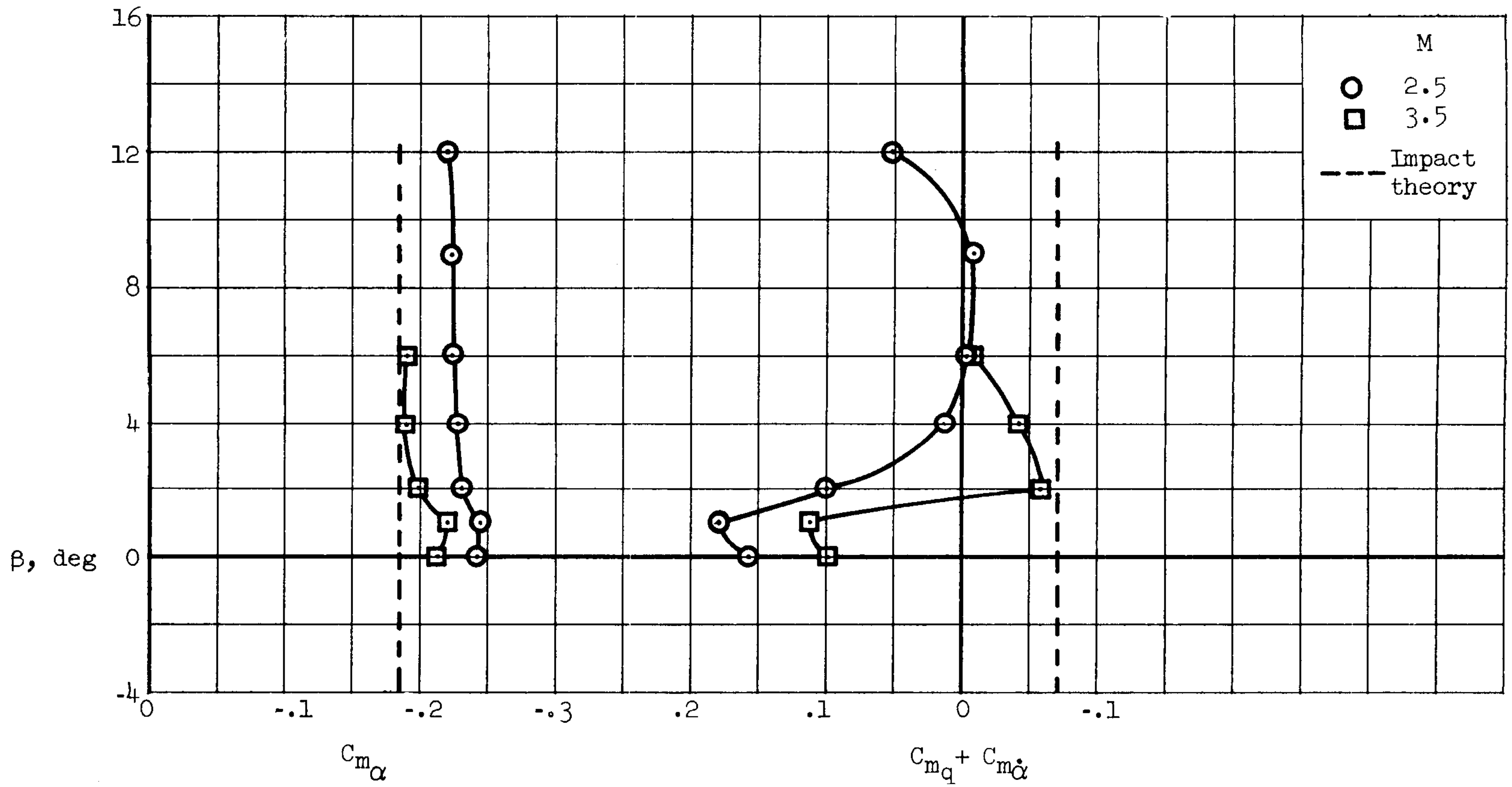

Figure 8.- Effect of variation in sideslip angle on the longitudinal dynamic stability derivative at zero angle of attack for the body of revolution having a flattened forebody (F_2A_2); moment center = 0.251D.

[redacted]

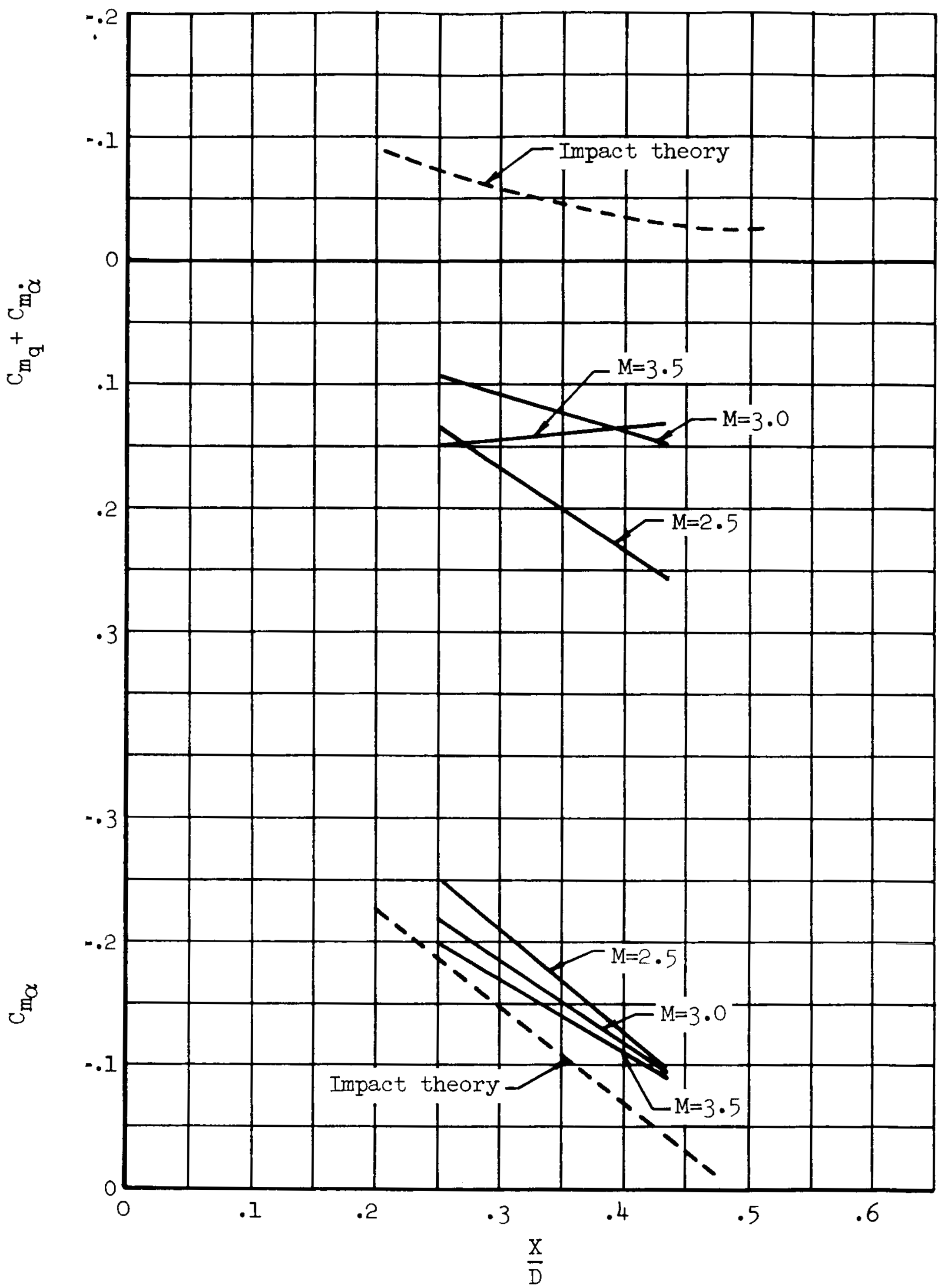

Figure 9.- The variation in static stability and damping in pitch with the location of the pitching axis for the body of revolution having a flattened forebody (F_2A_2) at $\alpha_m = 0^\circ$.

[redacted]

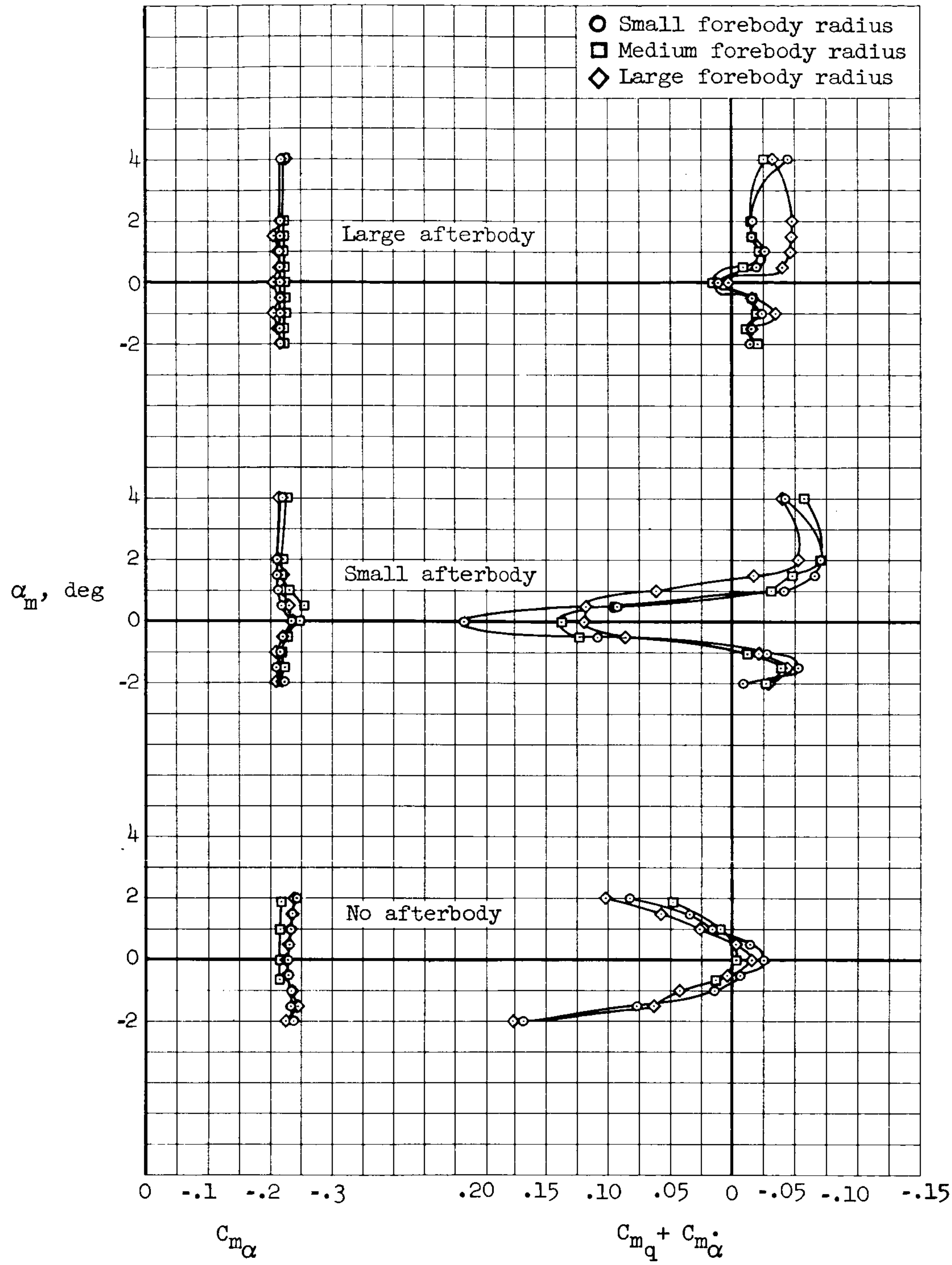

(a) M = 2.5

Figure 10.- Effect of shape variables (three afterbody configurations with each of three forebody configurations) on the flattened forebody with moment center located at 0.251D and having no forebody roughness.

[redacted]

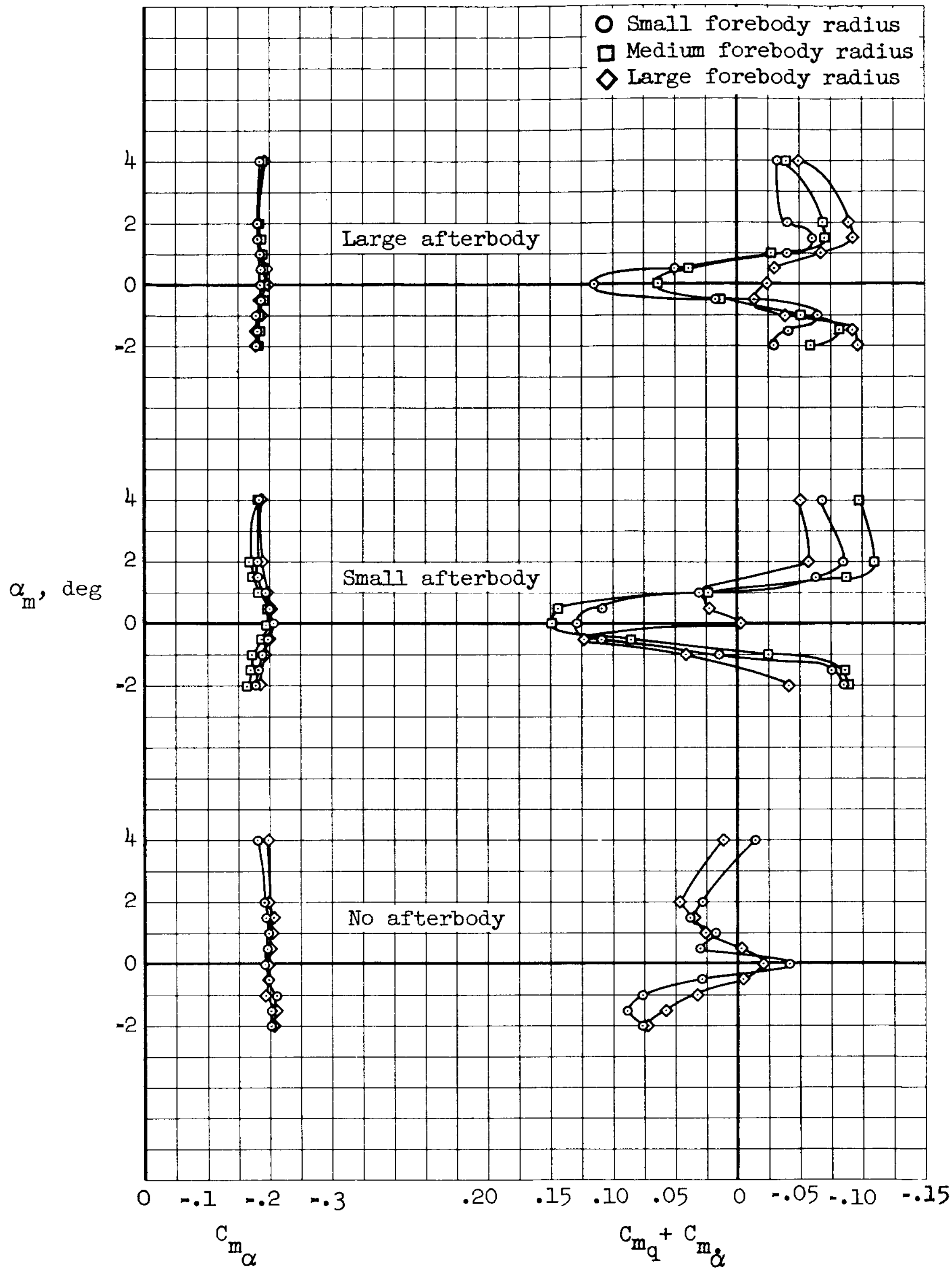

(b) M = 3.5

Figure 10.- Concluded.

[redacted]

[redacted]

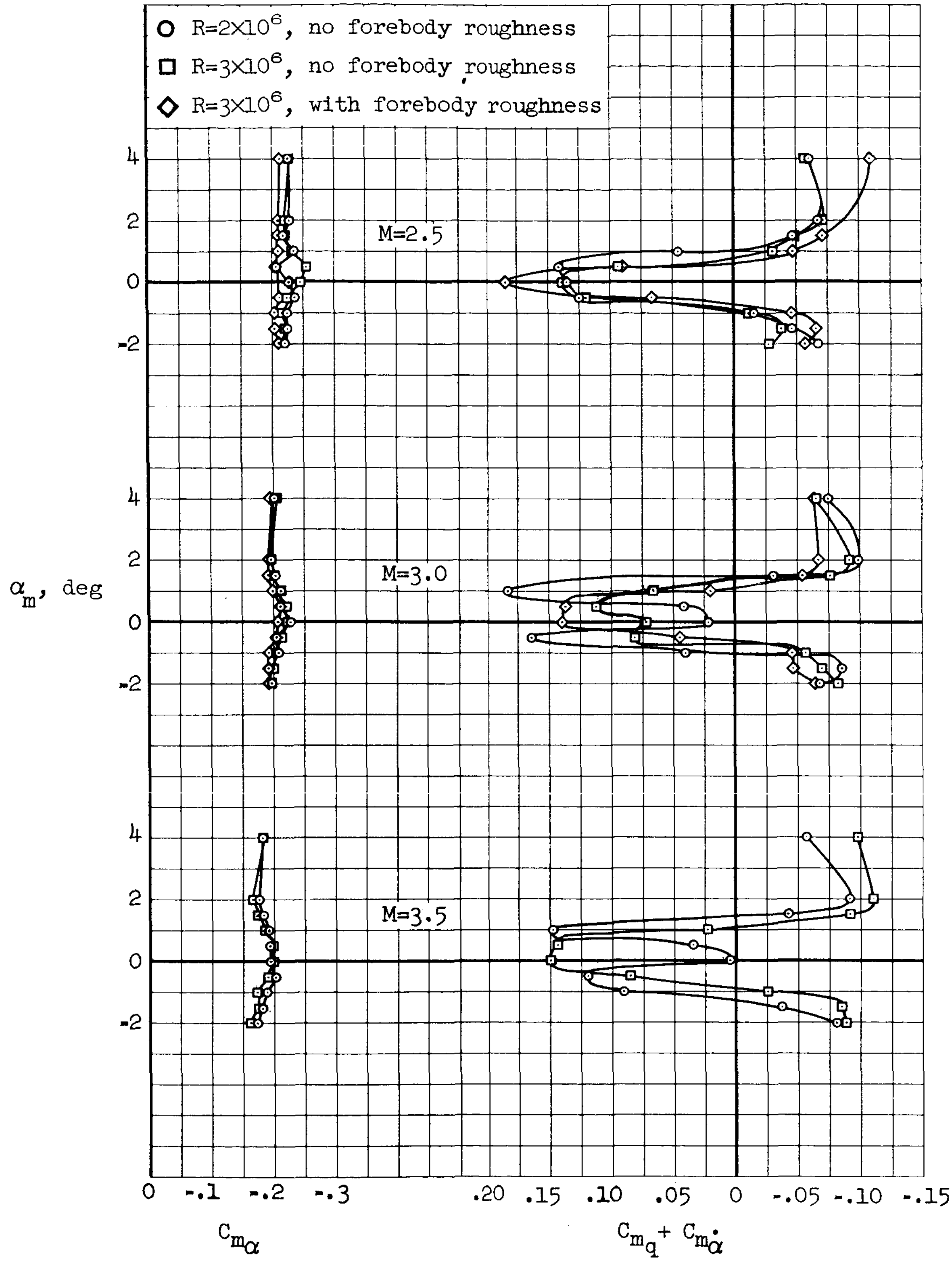

Figure 11.- Effect of Reynolds number and forebody roughness at three Mach numbers for the flattened forebody configuration with medium forebody radius and large afterbody; moment center = 0.251D.

[redacted]

[redacted]

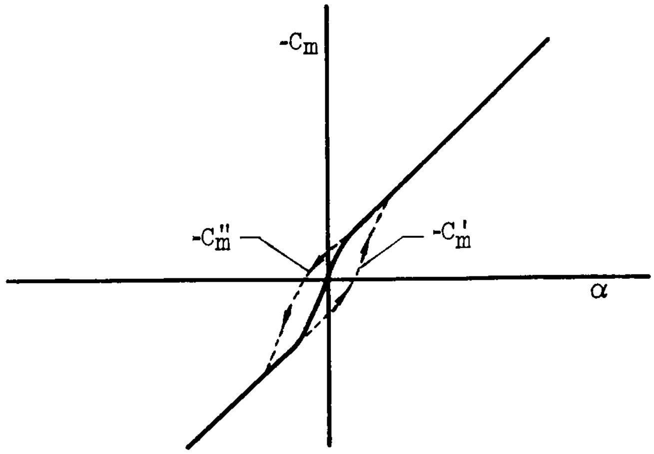

(a) C_m vs. α illustrating hysteresis.

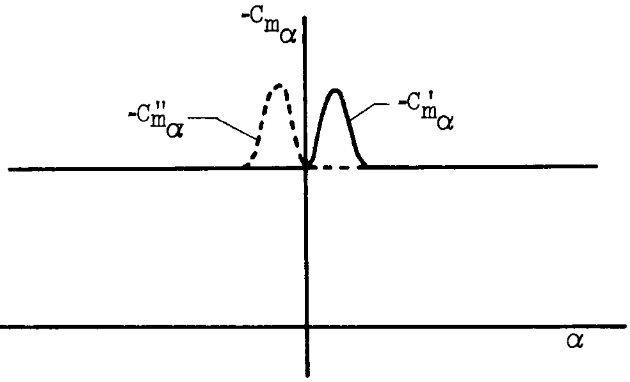

(b) Corresponding C_{m_α} vs. α.

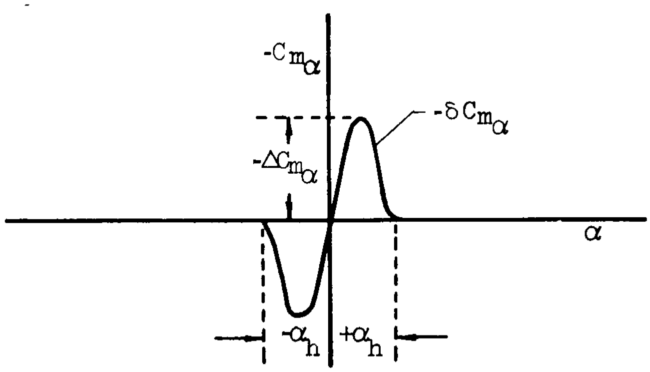

(c) ΔC_{m_α} vs. α corresponding to (a) and (b).

Figure 12.- Aerodynamic relations employed in evaluating effect of aerodynamic hysteresis on damping.

[redacted]

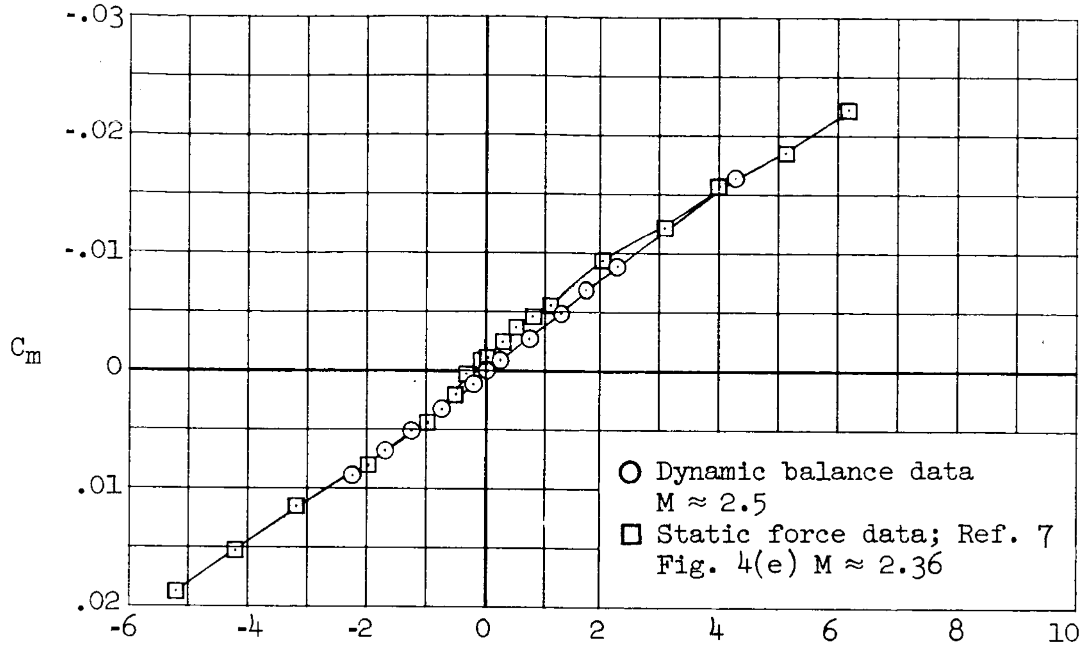

(a) M ≈ 2.5

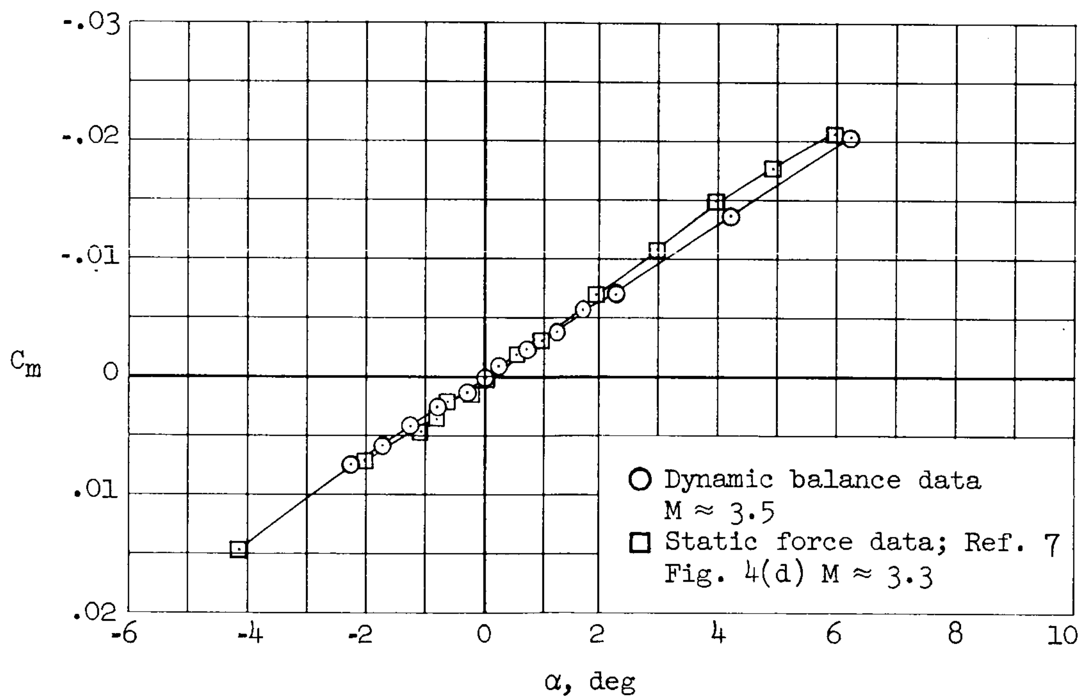

(b) M ≈ 3.5

Figure 13.- Variations of C_m vs. α compared with static-force data from reference 7 for the body of revolution having a flattened forebody with small afterbody and moment center at 0.251D.